PCCP

Accepted Manuscript

This is an *Accepted Manuscript*, which has been through the Royal Society of Chemistry peer review process and has been accepted for publication.

Accepted Manuscripts are published online shortly after acceptance, before technical editing, formatting and proof reading. Using this free service, authors can make their results available to the community, in citable form, before we publish the edited article. We will replace this *Accepted Manuscript* with the edited and formatted *Advance Article* as soon as it is available.

You can find more information about *Accepted Manuscripts* in the Information for Authors.

Please note that technical editing may introduce minor changes to the text and/or graphics, which may alter content. The journal's standard Terms & Conditions and the Ethical guidelines still apply. In no event shall the Royal Society of Chemistry be held responsible for any errors or omissions in this *Accepted Manuscript* or any consequences arising from the use of any information it contains.

ROYAL SOCIETY OF CHEMISTRY

www.rsc.org/pccp

Optimization of Al_2O_3/TiO_2 Nanolaminate Thin Films Prepared with Different Oxide Ratios, for use in Organic Light-Emitting Diode Encapsulation, via Plasma-Enhanced Atomic Layer Deposition

Lae Ho Kim[a], Yong Jin Jeong[a] , Tae Kyu An[b], Seonuk Park[a], Jin Hyuk Jang[a], Sooji Nam[c], Jaeyoung Jang[d*], Se Hyun Kim[e*], and Chan Eon Park[a*]

[a] Polymer Research Institute, Department of Chemical Engineering, Pohang University of Science and Technology, Pohang, 790-784, Republic of Korea. E-mail: cep@postech.ac.kr

[b] Department of Polymer Science and Engineering, Korea National University of Transportation, Chungju-si, Chungbuk, 380-702, Republic of Korea.

[c] Smart I/O Control Device Research Section, Electronics and Telecommunications Research Institute, Daejeon, 305-700, Republic of Korea.

[d] Department of Energy Engineering, Hanyang University, Seoul, 133-791, Republic of Korea. E-mail: jyjang15@hanyang.ac.kr

[e] School of Materials Science and Engineering, Yeungnam University, Gyeongsan, 38541, Republic of Korea. E-mail: shkim@yu.ac.kr

Abstract

Encapsulation is essential for protecting the air-sensitive components of organic light-emitting diodes (OLEDs), such as the active layers and cathode electrodes. Thin film encapsulation approaches based on an oxide layer are suitable for flexible electronics, including OLEDs, because they provide mechanical flexibility, the layers are thin, and they are easy to prepare. This study examined the effects of the oxide ratio on the water permeation barrier properties of Al_2O_3/TiO_2 nanolaminate films prepared by plasma-enhanced atomic layer deposition. We found that the Al_2O_3/TiO_2 nanolaminate film exhibited

Physical Chemistry Chemical Physics Accepted Manuscript

optimal properties for a 1:1 atomic ratio of Al_2O_3/TiO_2 with the lowest water vapor transmission rate of 9.16 x 10^{-5} g m^{-2} day^{-1} at 60˚C and 90% RH. OLED devices that incorporated Al_2O_3/TiO_2 nanolaminate films prepared with a 1:1 atomic ratio showed the longest shelf-life, in excess of 2,000 hours under 60˚C and 90% RH conditions, without forming dark spots or displaying edge shrinkage.

Keywords

Al_2O_3, TiO_2, plasma-enhanced atomic layer deposition (PEALD), thin film encapsulation (TFE), organic light-emitting diodes (OLEDs), nanolaminate films.

Physical Chemistry Chemical Physics Accepted Manuscript

1. INTRODUCTION

Organic light-emitting diodes (OLEDs) have gained considerable attention as one of the most promising candidates for use in future flexible displays and illumination technologies because their power consumption requirements are low, they are thin, lightweight, and mechanically flexible, they illuminate across a wide viewing angle, and their response time is fast.[1-4] The poor environmental stabilities of OLEDs, however, have presented an important barrier to commercialization because OLEDs tend to be vulnerable to moisture and oxygen damage. Cathode electrodes based on low work function metals and small molecule active layers are easily oxidized, delaminated, and/or crystallized upon exposure to water and oxygen.[5-7] These types of defects introduce dark spots and/or edge shrinkage in the emitting areas of the OLEDs. The OLEDs must, therefore, be appropriately encapsulated to prevent the penetration of water and oxygen molecules into the devices. The water vapor transmission rate (WVTR) is an important figure of merit for an encapsulation layer's barrier performance because water molecules affect an organic device more significantly than oxygen molecules. Generally, a WVTR level of about 10^{-6} g m^{-2} day^{-1} is required for stable OLED operation.[8]

Current OLED platform designs encapsulate the active device using glass or metal lids held together using a suitable adhesive to bring the WVTR value below 10^{-6} g m^{-2} day^{-1}, however, such rigid encapsulation materials are incompatible with fully flexible display applications, which represent the future of OLED research. Rigid glass substrates should ideally be replaced with flexible substrates to both passivate the devices and realize flexible OLEDs. Polymer substrates offer good candidate materials, but most polymer substrates show poor thermal stability and a high permeability to water with WVTR values of $1\text{-}10^{2}$ g m^{-2} day^{-1}.[9] There is an urgent need to develop gas permeation barrier films for polymer substrates and OLEDs with low processing temperature requirements.

Thin film encapsulation (TFE) offers a promising approach to passivating flexible electronics. It has been performed with various low temperature deposition techniques such as sputtering[10-12], plasma enhanced chemical vapor deposition (PECVD)[13-16], atomic layer deposition (ALD)[17-19], and plasma enhanced ALD (PEALD) processes[20-21]. In particular, the deposition technique can affect significantly barrier properties of gas permeation barrier films. Thus, solution processing and physical vapor deposition (PVD) techniques are not sufficient

Physical Chemistry Chemical Physics Accepted Manuscript

for OLED encapsulations without additional processes because of lower step coverage and relatively loosely packed microstructure[22-26]. In the case of inorganic single layer, typically reported WVTR values of barrier films deposited with ALD-based technique and the other processes are about 10^{-4} g m^{-2} day^{-1} and 10^{-1}-10^{-3} g m^{-2} day^{-1}, respectively.[10-26]

Among the various TFE methods, Atomic layer deposition (ALD) and plasma-enhanced ALD (PEALD) remain leading options because they produce pinhole-free, highly uniform, conformal films at low temperatures (< 100˚C) with atomic-scale thickness control.[27-28] Compared to thermal ALD, PEALD requires much shorter deposition times due to the short purging time and high reactivity of the O_2 plasma.[29-31] The O_2 plasma applied during the PEALD process does not significantly degrade the underlying devices or substrates because the plasma exposure time is short, and initial layers can protect against follow-up plasma reactions.[30] Therefore, PEALD offers unique advantages as a TFE technique for use in flexible OLED devices.

The most widely used materials for TFE are Al_2O_3, TiO_2, ZrO_2, SiO_2, and Si_3N_4 because they provide excellent gas barrier properties. Al_2O_3 thin films satisfy many of the requirements for a passivation layer in that they provide a high gas barrier performance, good thermal and mechanical stabilities, a high optical transmittance, and good adhesion to a variety of substrates, however, low-temperature processed Al_2O_3 thin films are generally amorphous with a low chemical stability, and the barrier performance deteriorates under high humidity conditions.[20] The deposition of alternating inorganic nanolayers (nanolaminate structures) has emerged as a possible solutions to overcoming the above-mentioned issues. Nanolaminate films provide a WVTR value that is much lower than the values obtained from single inorganic layers due to the high packing densities of the materials at the nanolayer interfaces. In a previous report, we showed that Al_2O_3/TiO_2 nanolaminate films exhibited a high packing density and good water resistance with a low WVTR value of 1.81 x 10^{-4} g m^{-2} day^{-1} at 60˚C and 90% relative humidity (RH) conditions. The nanolaminate films have been used successfully as a passivation layer for organic field-effect transistors, which has improved the device stability.[20] The WVTR value of 1.81 x 10^{-4} g m^{-2} day^{-1}, however, is not sufficiently low for OLED applications, and further reductions would be needed. In general, the barrier performance tends to improve as the number of interfaces present in the

Physical Chemistry Chemical Physics Accepted Manuscript

nanolaminate films increases.[19] Efforts to engineer the interface between Al_2O_3 and TiO_2 may yield further reductions in the WVTR values in Al_2O_3/TiO_2 nanolaminate films.

The present work describes the development of a PEALD-based Al_2O_3/TiO_2 nanolaminate thin film with enhanced water barrier properties via optimization of the Al_2O_3 and TiO_2 oxide ratio under controlled PEALD cycles. Subnanometer thick layers of Al_2O_3 and TiO_2 were alternately deposited to obtain an $AlTi_xO_y$ mixed phase across the entire film area. The atomic ratios measured from the Al_2O_3/TiO_2 nanolaminate films agreed well with sublayer thickness ratio. The WVTR values of the Al_2O_3/TiO_2 nanolaminate films were measured using a Ca test and the optimized Al_2O_3/TiO_2 nanolaminate films exhibited a lower WVTR value of 9.16×10^{-5} g m^{-2} day^{-1}. The nanolaminate films were successfully used as encapsulation layers in OLEDs without the need for additional layers. OLED devices prepared using the optimized nanolaminate passivation layers showed extended shelf-lives exceeding 2,000 hours under high temperature and humidity conditions (60˚C and 90% RH) without the formation of dark spots or edge shrinkage.

Physical Chemistry Chemical Physics Accepted Manuscript

Physical Chemistry Chemical Physics Accepted Manuscript

2. EXPERIMENTAL SECTION

The deposition of Al_2O_3 and TiO_2 films and Al_2O_3/TiO_2 nanolaminate films

Al_2O_3, TiO_2 films and Al_2O_3/TiO_2 nanolaminate films were grown on various substrates using 6 inch PEALD reactor (LTSR-150, Leintech). PEALD-based films were deposited onto a p-type Si (100) wafer, soda lime glass, polyethylene naphthalate (PEN), or OLED devices to investigate the chemical, physical, and water permeation barrier properties of the films after cleaning. The OLED devices, however, were not submitted to the cleaning process. The Si wafer and glass were cleaned sequentially with acetone and isopropyl alcohol in an ultrasonic bath for 20 min, dried using a N_2 blower, and exposed to UV radiation for 20 min to remove carbon contaminants. The PEN substrate was washed with isopropyl alcohol alone for 1 min and then exposed to UV radiation for 5 min after drying under a N_2 stream to prevent solvent-derived or UV degradation. The substrates were fixed onto 6 inch Si wafers using imide tape prior to the deposition step. The PEALD substrate heater and warm wall of the reactor were maintained at 100˚C and 80˚C, respectively. The samples were placed onto the PEALD substrate heater for 30 min to permit thermal equilibration between the PEALD substrate heater and the samples. The base pressure and processing pressure inside the reactor were 0.01 Torr and 0.5 Torr, respectively. The precursors to Al_2O_3 and TiO_2 were trimethylaluminum (TMA, Lake LED Materials) and tetrakis(dimethylamino)-titanium (TDMAT, EG Chem), respectively. The precursors were injected into the reaction chamber without a carrier gas. O_2 plasma was used as oxygen source with a 100 W radio frequency (RF) plasma power in all PEALD processes. The temperature of the canister containing the TMA source was maintained at room temperature. The sequence of pulses applied during one cycle of Al_2O_3 layer deposition consisted of the TMA feeding (0.1 s), Ar purging (10 s), O_2 feeding (1.5 s), O_2 feeding with RF plasma (3 s), and Ar purging (10 s). The temperature of the canister containing the TDMAT source was maintained at 60˚C using a heating system to increase the vapor pressure. The sequence of pulses applied over one cycle of TiO_2 layer deposition consisted of TDMAT feeding (1 s), Ar purging (10 s), O_2 feeding (1.5 s), O_2 feeding with RF plasma (3 s), and Ar purging (10 s). Al_2O_3/TiO_2 nanolaminate films were fabricated simply to control the number of Al_2O_3 or TiO_2 PEALD cycles and an Al_2O_3 layer was deposited first.

Preparation of the Ca test cell

We prepared a calcium (Ca) test cell in order to determine the WVTR value for the barrier film prepared on PEN substrate. Aluminum (Al) and Ca (20 x 20 mm^2) were deposited in that order onto glass plates (50 x 50 mm^2) to produce films 120 nm and 250 nm thick, respectively, using a thermal evaporator under high vacuum (5 x 10^{-6} Torr). A patterned Al electrode was connected to the Ca layer for the conductance measurements. The Ca film was subsequently encapsulated using a PEALD barrier-coated PEN substrate (125 μm thick) using a UV-curable sealant (XNR 5570-B1, Nagase ChemteX). Four-point conductance measurements (GDM-8255A. GW INSTEK) were made to determine the conductance changes in the Ca layers over time under accelerated aging conditions (60˚C and 90% RH). The initial conductance value of Ca in the cell was 1.95 ± 0.34 S.

OLED fabrication and thin film encapsulation

The OLEDs were fabricated using an octagonal cluster-type thermal evaporating system (SUNCICEL 0603, SUNIC) under a vacuum of less than 5 x 10^{-6} Torr without breaking the vacuum. The indium tin oxide (ITO) patterned glass substrates, with a sheet resistance of 12 Ω sq^{-1} that had been photoresist (PR)-patterned to define the 2 x 2 mm^2 emitting area were used to form a bottom emission-type OLED device. Prior to depositing the organic materials, the ITO substrate was cleaned using the Si wafer cleaning process described above. After applying UV irradiation to the cleaned ITO substrate for 20 min, organic active layers and a metallic cathode were deposited in the configuration of MoO_3 (3 nm) as the hole injection layer / a-naphthylphenylbiphenyl (NPB) (50 nm) as a hole transport layer / 10-(2-benzothiazolyl)-2,3,6,7-tetrahydro-1,1,7,7-tetramethyl-1H,5H,11H-(1)-benzopyropyrano(6,7-8-I,j)quinoizin-11-one (C545T) 2% doped tris(8-quinolato)aluminum (Alq_3) (30 nm) as an emitting layer / Alq_3 (20 nm) as an electron transport layer / quinolato lithium (Liq) (1 nm) as an electron injection layer / Al (120 nm) as a cathode. After OLED fabrication, glass encapsulation was performed in a glove box using a UV curable epoxy with a moisture adsorbent. Thin film encapsulation was achieved by transferring the vacuum-packaged OLED

Physical Chemistry Chemical Physics Accepted Manuscript

devices into a glove box connected to PEALD equipment and depositing the oxide films onto OLED devices directly without applying pretreatment or buffer layers.

Thin films and devices characterization

The thicknesses and refractive indices of the PEALD films prepared on the Si wafers were measured using a spectroscopic ellipsometer (M-2000, J.A.Woollam). The optical transmittance values of the PEALD films on glass were measured using a UV-Vis spectrometer (V-670, Jasco) over the wavelength range 400-800 nm. The chemical compositions and film density were characterized using X-ray photoelectron spectroscopy (XPS, Yeungnam University Center for Research Facilities) and X-ray reflectivity measurements (XRR, the Korea Basic Science Institute in Korea), respectively. The crystallinities of the PEALD films on a Si wafer were determined from the X-ray diffraction patterns (XRD, collected at the 5A beamline at the Pohang Accelerator Laboratory in Korea).

The current density, voltage, and luminescence (*J*-*V*-*L*) characteristics were measured using a current source meter (236, Keithley) and a luminescence meter (CS1000, Minolta) under ambient conditions (25˚C and 50% RH). The shelf-lives of the OLEDs were tested after storage in a 60˚C, 90% RH climate chamber, and the emitting areas were imaged using a CCD camera at appropriate intervals.

Physical Chemistry Chemical Physics Accepted Manuscript

3. RESULTS AND DISCUSSION

Characterization of the Al_2O_3/TiO_2 nanolaminate films

Al_2O_3/TiO_2 nanolaminate films with PEALD cycle ratios of 4/1, 3/1, 1/1, 1/3, and 1/7 were prepared at different oxide ratios, and single Al_2O_3 and TiO_2 films were also grown as references at a deposition temperature of 100˚C. The sublayer thickness obtained per PEALD cycle was 1.8 Å $cycle^{-1}$ for Al_2O_3 and 0.75 Å $cycle^{-1}$ for TiO_2. This value is in good agreement with the growth rate reported by other gropus.[32-34] The thicknesses of all PEALD films, including the nanolaminate films, agreed well with the target thicknesses within an error range of 2.14%. For brevity, an Al_2O_3/TiO_2 nanolaminate film consisting of 4 cycles of Al_2O_3 and 1 cycle of TiO_2, is referred to as "A4T1". We confirmed the compositions of nanolaminate films using quantitative XPS analysis (see the Supporting Information Figure S1, which presents the XPS spectra of Al_2O_3, TiO_2, and Al_2O_3/TiO_2 nanolaminate films at the Al 2p and Ti 2p core levels). The composition ratios were compared with the sublayer thickness ratios, as presented in Fig. 1. The atomic ratio agreed well with the sublayer thickness ratio, indicating that the atomic ratio could be easily controlled by adjusting the number of PEALD cycles applied.

The refractive index and optical transmittance values of the 50 nm thick PEALD-based films are shown in Fig. 2 and are summarized in Table 1. As the fraction of TiO_2 increased the refractive index increased, and the optical transmittance decreased. The refractive index values at 550 nm were 1.64 and 2.45 for the single Al_2O_3 and TiO_2 film, respectively. The PEALD-based films displayed refractive index values that exceeded those measured from the thermal ALD films, possibly due to low defect densities.[35] The UV-Vis spectra were collected to determine the optical transmittance from 400 nm to 800 nm. As shown in Fig. 2b and Table 1, the average visible transmittance values ontained from the PEALD-based films, including the TiO_2 film, exceeded 70%. Despite the large refractive index difference between Al_2O_3 and TiO_2, no interference was observed. These results indicated that Al_2O_3 and TiO_2 mixed well when alternately deposited as atomic-scale sublayers without forming a crystalline phase (see the Supporting Information Figure S2, which provides the XRD spectra of the Al_2O_3, TiO_2, and Al_2O_3/TiO_2 nanolaminate films). The relatively lower transmittance values of nanolaminate films resulting from the addition of TiO_2 could be ameliorated by reducing the

Physical Chemistry Chemical Physics Accepted Manuscript

total film thickness (see the Supporting Information Figure S3, the optical transmittance spectra of the A1T3 film prepared in various thicknesses). The dielectric constant was readily adjusted by varying the number of applied PEALD cycles as well as the optical parameters (see the Supporting Information Table S1, the dielectric constants of the Al_2O_3, TiO_2, and Al_2O_3/TiO_2 nanolaminate films).

Gas permeation barrier properties of the PEALD-based films

The WVTR values for the barrier films were determined using the Ca test. We deposited 50 nm thick PEALD-based films on PEN substrate due to obtain saturated WVTR value with sufficient flexibility (see the Supporting Information Figure S4, optical microscope images for PEALD-based films on PEN substrate after 500 times cyclic bending test with a bending radius of 22 mm). Generally, the WVTR values are saturated for films thicker than 20 nm.[36-37] Figure 3 shows a schematic diagram of the Ca test used in this study. A 250 nm thick Ca film was overlapped with Al electrodes and encapsulated with a barrier film on a PEN substrate using epoxy glue. The water vapor permeability of the barrier-coated polymer film itself was determined without directly depositing a barrier layer onto Ca. The conductance of Ca decreased over time as the chemical reaction of Ca with water vapor or/and oxygen proceeded [$Ca + 2H_2O \rightarrow Ca(OH)_2 + H_2$, $2Ca + O_2 \rightarrow 2CaO$]. The WVTR measurements were collected in a climate chamber under 60˚C and 90% RH accelerated aging conditions, the reaction of Ca and water was presumed to dominate the reaction rate. The WVTR values of the barrier-coated PEN were calculated according to the following equation.[38]

$$\mathrm{WVTR}\ [\mathrm{g\ m^{-2}\ day^{-1}}] = -\ n \cdot (M_{H2O} / M_{Ca}) \cdot \rho_{Ca} \cdot \sigma_{Ca} \cdot [d(1/R)/dt] \cdot (S_{Ca} / S_{window}),$$

where n is the molar equivalent of the degradation reaction [$n=2$, $Ca + 2H_2O \rightarrow Ca(OH)_2 + H_2$], M_{H2O} and M_{Ca} are the molecular weights of H_2O (18 g mol^{-1}) and Ca (40.1 g mol^{-1}), respectively, ρ_{Ca} and σ_{Ca} are the density (1.55 g cm^{-3}) and resistivity ($3.4 \cdot 10^{-8}$ Ωm) of Ca, respectively, S_{Ca} is the area of Ca (20 x 20 mm^2) and S_{window} is the transmission area of the water vapor (26 x 26 mm^2). The conductance change, $d(1/R)/dt$, was calculated based on the slope of the Ca test plot between 24 and 36 hours to avoid the initial fluctuations in the Ca resistance due to the outgassing of residual gases from the epoxy glue and the equilibration of

Physical Chemistry Chemical Physics Accepted Manuscript

the climate chamber after introduction to the 60˚C and 90% RH conditions. The fluctuations in the Ca resistance were observed for 24 hours from the start of the study. The epoxy sealing degraded after 50 hours under the accelerated aging conditions (see the Supporting Information Figure S5b, which plots the WVTR value of the glass-encapsulated Ca test cell as a function of time, during incubation at 60˚C and 90% RH). As shown in Fig 3b, the conductance decreased with the measurement time due to Ca corrosion. Al_2O_3/TiO_2 nanolaminate films exhibited a slower decrease in the rate of conductance compared to the single Al_2O_3 or TiO_2 films. The WVTR values of the PEALD-based barrier films on the PEN substrates are summarized in Table 1. The A1T3 film showed the lowest WVTR value of 9.16 x 10^{-5} g m^{-2} day^{-1}. This WVTR value was about 5 x 10^{3} times better than that of the bare PEN substrate with a WVTR value of 5.20 x 10^{-1} g m^{-2} day^{-1}. This value was comparable to the value obtained from the glass-encapsulated Ca test cell, with a WVTR value of 4.35 x 10^{-5} g m^{-2} day^{-1} (see the Supporting Information Figure S5, normalized conductance change, and WVTR value of the glass-encapsulated Ca test cell as function of time at 60˚C and 90% RH).

Characteristics of the OLED devices passivated with PEALD-based films

The current density, voltage, and luminescence (*J-V-L*) were measured to permit a comparison of the electrical behaviors of the OLEDs before and after passivation. Figure 4 shows the typical *J-V-L* characteristics of the OLED devices passivated with 50 nm thick PEALD films at a deposition temperature of 100˚C. The *J-V-L* values of the glass-encapsulated devices were measured for reference purposes. As shown in Fig. 4, the current density and luminance values obtained from the PEALD-processed devices were smaller than those of the glass-encapsulated devices at the same voltage. We expected that this degree of degradation mainly arose from heating during the process. The deterioration of the devices was severe after longer periods of exposure to heat at 100˚C, however, O_2 plasma damage was not considered because the PEALD process, which involves a short plasma exposure time and large intervals between the O_2 plasma steps, has little influence on the substrate.[7, 39] The glass-encapsulated devices were annealed on a 100˚C hot plate for 4, 6, and 24 hours to compare the heating effects in the PEALD-processed devices. The PEALD oxide-passivated devices were exposed to heat at 100˚C for 4-12 hours, including the deposition time. The

Physical Chemistry Chemical Physics Accepted Manuscript

trends in the current density and luminance reduction in the glass-encapsulated devices were similar to those observed in the PEALD oxide-passivated devices.

Hole-only device characteristics

The OLED device degradation after application of the PEALD process was attributed to a drop in the hole mobility as a result of crystallization of the NPB layer becuase the glass transition temperature (T_g) of NPB was less than 100˚C (NPB: T_g = 90-95˚C, Alq_3: Tg = 150˚C).[40-41] The effects of thermal annealing were further studied by measuring the *J-V* characteristics of hole-only devices with or without a PEALD-based passivation layer. The device structure was ITO / MoO_3 (3 nm) / NPB (200 nm) / Al (120 nm) / passivation layer (50 nm). Glass-encapsulated hole-only devices were annealed on a hot plate at 100˚C for 4 hours, and the PEALD barrier-coated hole-only devices were annealed at the same temperature for 4 hours, including the deposition time. Figure 5 shows that the current densities of all annealed devices decreased relative to the values measured from the non-annealed devices. The small difference in the current densities of the glass-encapsulated device and the PEALD film-passivated devices may have resulted from a disparity in the actual temperatures of each heater.

Interestingly, the current efficiency in the device prepared using PEALD exceeded the current efficiency measured from the bare device. The current efficiency enhancement could be explained as resulting from improved carrier balancing in the devices due to the annealing process (see the Supporting Information Figure S6, current efficiency for the glass-encapsulated devices and the devices passivated with PEALD films). As the holes are the majority carrier in the NPB / Alq_3-based OLEDs, a decrease in the hole mobility in the NPB film produced a comparable decrease in the hole current, leading to greater balance between the electron and hole carriers. This effect clearly improved the device performance.[42] A reduction in hole carriers in the Alq_3 layer could retard the device degradation process. Aziz et al. showed that the hole carrier in Alq_3 contributes significantly to device degradation. It is reasonable to expect that devices deposited at high substrate temperatures may offer better performances due to their reduced hole current.[43]

Physical Chemistry Chemical Physics Accepted Manuscript

Physical Chemistry Chemical Physics Accepted Manuscript

Shelf-lives of the OLED devices

The lifetimes of OLED devices prepared with or without 50 nm thick PEALD-based passivation layers were characterized as a function of time using the shelf-life test instead of the constant current driving measurements because the current efficiency varied from OLED device to device. The devices were stored under the conditions used in the Ca test (a 60˚C 90% RH climate chamber) and were imaged at 65 μA in appropriate intervals as shown in Fig 6. The initial luminance and voltage at 65 μA were 200 ± 15 cd m^{-2} and 4.14 ± 0.23 V, respectively. The shelf-lives, defined as the time within which the emitting area (2 x 2 mm^2) was reduced by one-half, were 1136 hours for the single Al_2O_3 and TiO_2, 1632 hours for A3T1 and A4T1, and more than 2000 hours for A1T1, A1T3, and A1T7. The emitting area of each OLED device was calculated using the Image J program, as depicted in Fig 7. The A1T3-passivated OLED device, in particular, retained its initial emitting area until 2000 hours, in good agreement with the lowest WVTR value obtained from the Ca test.

The excellent water permeation barrier properties of the A1T3 film could be explained in terms of the following effects. First, the addition of TiO_2 to the Al_2O_3 matrix resulted in the formation of relatively strong Al-O-Ti bonds that improved the chemical resistance of the material, as mentioned in previous reports.[20] We evaluated the water resistance by measuring the refractive index change over time in the PEALD-based films upon immersion in water at room temperature. The refractive index of the Al_2O_3 film decreased rapidly after 29 hours due to the porous structure of the film, however, the A4T1 film, which included the lowest TiO_2 content tested in this study, showed an even smaller change, a decrease of 2.14% of the initial value, over 2100 hours (see the Supporting Information Figure S7, which plots the refractive indices of the PEALD-based films on a Si wafer over time in water at room temperature). Second, the highly packed $AlTi_xO_y$ mixed phase reduced the water permeability. Meyer et al. reported that $ZrAl_xO_y$ aluminate phases in the interface regions of the Al_2O_3/ZrO_2 nanolaminate films were thermodynamically stable and offered a high packing density.[44] Seo et al. reported the measurement of a reduction in the WVTR value as the number of interfaces increased in the Al_2O_3/ZrO_2 nanolaminate film.[19] The $AlTi_xO_y$ mixed phase was stable and characterized by a high packing density.[20, 45-46] Sintonen et al. reported that a single $AlTi_xO_y$

layer could be obtained by the alternate deposition of Al_2O_3 and TiO_2 films with a thickness of less than each monolayer thickness, which could obtained from the density value. The monolayer thicknesses of Al_2O_3 and TiO_2 films were estimated based on the film density.[27] XRR measurements were used to determine the film densities: 3.00 g cm^{-3} for Al_2O_3 and 3.85 g cm^{-3} for TiO_2 with a thickness of 50 nm at deposition temperature of 100˚C. The estimated monolayer thicknesses of the Al_2O_3 and TiO_2 were 3.84 Å and 3.25 Å, respectively. The A1T1 and A1T3 films, which consisted of Al_2O_3 and TiO_2 deposited alternately to film thicknesses of less than the monolayer thicknesses for both Al_2O_3 and TiO_2, was expected to functionally resemble a composite film. The A1T3 film was expected to provide the largest Al-O-Ti bond and the highest packing density due to the 1:1 atomic ratio of Al_2O_3 and TiO_2.

Physical Chemistry Chemical Physics Accepted Manuscript

4. CONCLUSIONS

In summary, we developed Al_2O_3/TiO_2 nanolaminate films with different oxide ratios by using the PEALD technique. The atomic ratio in the nanolaminate films could be readily controlled by adjusting the number of PEALD cycles applied. The Al_2O_3/TiO_2 nanolaminate films were deposited onto polymer and OLED devices in an effort to optimize the water permeation barrier properties of these films. The nanolaminate films exhibited better barrier functions than the single Al_2O_3 or TiO_2 films. The 50 nm thick A1T3 film with a sublayer thickness ratio of about 1:1 for Al_2O_3/TiO_2 exhibited the lowest WVTR value of 9.16 x 10^{-5} g m^{-2} day^{-1} at 60˚C and 90% RH accelerated aging conditions. The OLED device passivated with an A1T3 layer and a thickness of only 50 nm showed the longest shelf-life, exceeding 2,000 hours at 60˚C and 90% RH, without forming any dark spots or edge shrinkage. We expected that a lower sublayer thickness and a 1:1 atomic ratio were needed to obtain the highest packing density with a sufficient chemical resistance in the Al_2O_3/TiO_2 nanolaminate system.

AUTHORINFORMATION

Corresponding Author

*E-mail: cep@postech.ac.kr, Fax: +82-54-279-8298, Tel: +82-54-279-2269 (C. E. Park)

*E-mail: shkim97@yu.ac.kr, Fax: +82-54-810-4686, Tel: +82-53-810-2779 (S. H. Kim)

*E-mail: jyjang15@hanyang.ac.kr, Fax: +82-2-2220-2334, Tel: +82-2-2291-5982 (J. Jang)

ACKNOWLEDGMENTS

This study was supported by a grant from the National Research Foundation of Korea (NRF), funded by the Korean Government (MSIP NRF-2014R1A2A1A05004993), and by the New & Renewable Energy of the Korea Institute of Energy Technology Evaluation and

Physical Chemistry Chemical Physics Accepted Manuscript

Planning (KETEP) grant funded by the Korean Government through the Ministry of Knowledge Economy (no. 20123010010140). This research was also supported by the Samsung Display Corporation.

References

1. N. Thejo Kalyani and S. J. Dhoble, *Renew. Sustain. Energy Rev.*, 2012, **16**, 2696–2723.

2. T.-H. Han, Y. Lee, M.-R. Choi, S.-H. Woo, S.-H. Bae, B. H. Hong, J.-H. Ahn and T.-W. Lee, *Nat. Photonics*, 2012, **6**, 105–110.

3. H. Sasabe and J. Kido, *J. Mater. Chem. C*, 2013, **1**, 1699–1707.

4. S. Kunić and Z. Šego, *Proc. ELMAR*, 2012, 31-35.

5. M. Schaer, F. Nüesch, D. Berner, W. Leo and L. Zuppiroli, *Adv. Funct. Mater.*, 2001, **11**, 116–121.

6. H. Aziz, Z. Popovic, S. Xie, A.-M. Hor, N.-X. Hu, C. Tripp and G. Xu, *Appl. Phys. Lett.*, 1998, **72**, 756–758.

7. S. Park, W. M. Yun, L. H. Kim, S. Park, S. H. Kim and C. E. Park, *Org. Electron.*, 2013, **14**, 3385–3391.

8. M. S. Weaver, L. A. Michalski, K. Rajan, M. A. Rothman, J. A. Silvernail, J. J. Brown, P. E. Burrows, G. L. Graff, M. E. Gross, P. M. Martin, M. Hall, E. Mast, C. Bonham, W. Bennett and M. Zumhoff, *Appl. Phys. Lett.*, 2002, **81**, 2929–2931.

9. J. S. Lewis and M. S. Weaver, *IEEE J. Sel. Top. Quantum Electron.*, 2004, **10**, 45–57.

10. A. G. Erlat, B. M. Henry, C. R. M. Grovenor, A. G. D. Briggs, R. J. Chater and Y. Tsukahara, *J. Phys. Chem. B*, 2004, **108**, 883–890.

11. B. M. Henry, A. G. Erlat, A. McGuigan, C. R. M. Grovenor, G. A.D. Briggs, Y. Tsukahara, T. Miyamoto, N. Noguchi and T. Niijima, *Thin Solid Films*, 2001, **382**, 194–201.

12. J. Fahlteich, M. Fahland, W. Schönberger and N. Schiller, *Thin Solid Films*, 2009, **517**, 3075–3080.

13. P. F. Carcia, R. S. McLean, M. D. Groner, A. A. Dameron and S. M. George, *J. Appl. Phys.*, 2009, **106**, 23533.

14. D.-S. Wuu, T.-N. Chen, E. Lay, C.-H. Liu, C.-H. Chang, H.-F. Wei, L.-Y. Jiang, H.-U. Lee and Y.-Y. Chang, *J. Electrochem. Soc.*, 2010, **157**, C47-C51.

15. H.-K. Kim, S.-W. Kim, D.-G. Kim, J.-W. Kang, M. S. Kim and W. J. Cho, *Thin Solid Films*, 2007, **515**,

Physical Chemistry Chemical Physics Accepted Manuscript

4758–4762.

16. S. Zanini, C. Riccardi, M. Orlandi and E. Grimoldi, *Vacuum*, 2007, **82**, 290–293.

17. P. F. Carcia, R. S. McLean, M. H. Reilly, M. D. Groner and S. M. George, *Appl. Phys. Lett.*, 2006, **89**, 031915.

18. S.-W. Seo, H. Chae, S. J. Seo, H. K. Chung and S. M. Cho, *Appl. Phys. Lett.*, 2013, **102**, 161908.

19. S.-W. Seo, E. Jung, H. Chae and S. M. Cho, *Org. Electron.,* 2012, **13**, 2436–2441.

20. L. H. Kim, K. Kim, S. Park, Y. J. Jeong, H. Kim, D. S. Chung, S. H. Kim and C. E. Park, *ACS Appl. Mater. Interfaces*, 2014, **6**, 6731–6738.

21. H. Jung, H. Choi, H. Jeon, S. Lee and H. Jeon, *J. Appl. Phys.*, 2013, **114**, 173511.

22. S. Park, S. Nam, L. Kim, M. Park, J. Kim, T. K. An, W. M. Yun, J. Jang, J. Hwang and C. E. Park, *Org. Electron.*, 2012, **13**, 2786–2792.

23. J. Jin, J. J. Lee, B.-S. Bae, S. J. Park, S. Yoo and K. Jung, *Org. Electron.*, 2012, **13**, 53–57.

24. W. M. Yun, J. Jang, S. Nam, L. H. Kim, S. J. Seo and C. E. Park, *ACS Appl. Mater. Interfaces*, 2012, **4**, 3247–3253.

25. Y. C. Han, C. Jang, K. J. Kim, K. C. Choi, K. Jung and B.-S. Bae, *Org. Electron.*, 2011, **12**, 609–613.

26. W. M. Yun, J. Jang, S. Nam, Y. J. Jeong, L. H. Kim, S. Park, S. J. Seo and C. E. Park, *J. Mater. Chem.*, 2012, **22**, 25395.

27. S. M. George, *Chem. Rev.*, 2010, **110**, 111–131.

28. M. D. Groner, S. M. George, R. S. McLean and P. F. Carcia, *Appl. Phys. Lett.*, 2006, **88**, 51907.

29. S. Ozaki, T. Ohki, M. Kanamura, T. Imada, N. Nakamura, N. Okamoto, T. Miyajima and T. Kikkawa, *CS MANTECH Conf.*, 2012, 1–4.

30. S. J. Yun, J. W. Lim and J.-H. Lee, *Electrochem. Solid-State Lett.*, 2004, **7**, C13-C15.

31. S. E. Potts, W. Keuning, E. Langereis, G. Dingemans, M. C. M. van de Sanden and W. M. M. Kessels, *J. Electrochem. Soc.*, 2010, **157**, P66-P74.

32. E. Langereis, M. Creatore, S. B. S. Heil, M. C. M. Van De Sanden and W. M. M. Kessels, *Appl. Phys. Lett.*, 2006, **89**, 081915.

33. D. Cao, X. Cheng, L. Zheng, D. Xu, Z. Wang, C. Xia, L. Shen, Y. Yu and D. Shen, *J. Vac. Sci. Technol. B,* 2015, **33**, 01A101.

Physical Chemistry Chemical Physics Accepted Manuscript

34. Q. Xie, J. Musschoot, D. Deduytsche, R. L. Van Meirhaeghe, C. Detavernier, S. Van den Berghe, Y.-L. Jiang, G.-P. Ru, B.-Z. Li and X.-P. Qu, *J. Electrochem. Soc.*, 2008, **155**, H688.

35. G. Triani, P. J. Evans, D. R. G. Mitchell, D. J. Attard, K. S. Finnie, M. James, T. Hanley, B. Latella, K. E. Prince and J. Bartlett, *Proc. SPIE*, 2005, **5870**, 587009.

36. P. F. Carcia, R. S. McLean and M. H. Reilly, *Appl. Phys. Lett.*, 2010, **97**, 221901.

37. E. Langereis, M. Creatore, S. B. S. Heil, M. C. M. van de Sanden and W. M. M. Kessels, *Appl. Phys. Lett.*, 2006, **89**, 081915.

38. R. Paetzold, A. Winnacker, D. Henseler, V. Cesari and K. Heuser, *Rev. Sci. Instrum.*, 2003, **74**, 5147–5150.

39. S. J. Yun, Y. W. Ko and J. W. Lim, *Appl. Phys. Lett.*, 2004, **85**, 4896–4898.

40. G.-T. Chen, S.-H. Su, C.-C. Hou and M. Yokoyama, *J. Electrochem. Soc.*, 2007, **154**, J159-J162.

41. J. Cui, Q. Huang, J. C. G. Veinot, H. Yan, Q. Wang, G. R. Hutchison, A. G. Richter, G. Evmenenko, P. Dutta and T. J. Marks, *Langmuir*, 2002, **18**, 9958–9970.

42. M.-C. Sun, J.-H. Jou, W.-K. Weng and Y.-S. Huang, *Thin Solid Films*, 2005, **491**, 260–263.

43. H. Aziz, Z. D. Popovic and N.-X. Hu, *Appl. Phys. Lett.*, 2002, **81**, 370-372.

44. J. Meyer, P. Görrn, F. Bertram, S. Hamwi, T. Winkler, H. H. Johannes, T. Weimann, P. Hinze, T. Riedl and W. Kowalsky, *Adv. Mater.*, 2009, **21**, 1845–1849.

45. C. C. Chen, *Atlas J. Mater. Sci.*, 2014, **1**, 1–11.

46. P. Vitanov, A Harizanova, T. Ivanova and K. Ivanova, *J. Mater. Sci.*, 2003, **14**, 757–758.

Physical Chemistry Chemical Physics Accepted Manuscript

Physical Chemistry Chemical Physics Accepted Manuscript

Figure and Table captions

Figure 1. Comparison of the atomic ratio and sublayer thickness ratio in the PEALD-based films grown at 100˚C.

Figure 2. (a) The refractive index and (b) transmittance of the PEALD-based films prepared with a thickness of 50 nm.

Figure 3. (a) Schematic diagram showing the Ca test, and (b) normalized conductance changes in the Ca encapsulated with PEALD films on a PEN substrate at 60˚C and 90% RH.

Figure 4. (a) *J-V* and (b) *L-V* characteristics of the OLED devices prepared with PEALD-based passivation layers and glass-encapsulated devices. The inset shows a schematic configuration of the OLED.

Figure 5. *J-V* characteristics of hole-only devices prepared with and without PEALD-based passivation layers. The inset shows a schematic configuration of the hole-only device.

Figure 6. Shelf-life of the OLED devices passivated with and without PEALD-based films at 60˚C and 90% RH.

Figure 7. The emitting area over time, measured in OLED devices passivated with or without PEALD-based films at 60˚C and 90% RH.

Table 1. Refractive index at 550 nm, the average optical transmittance across the visible region (400 nm–800 nm), and WVTR values of the PEALD-based films.

Figure and Table

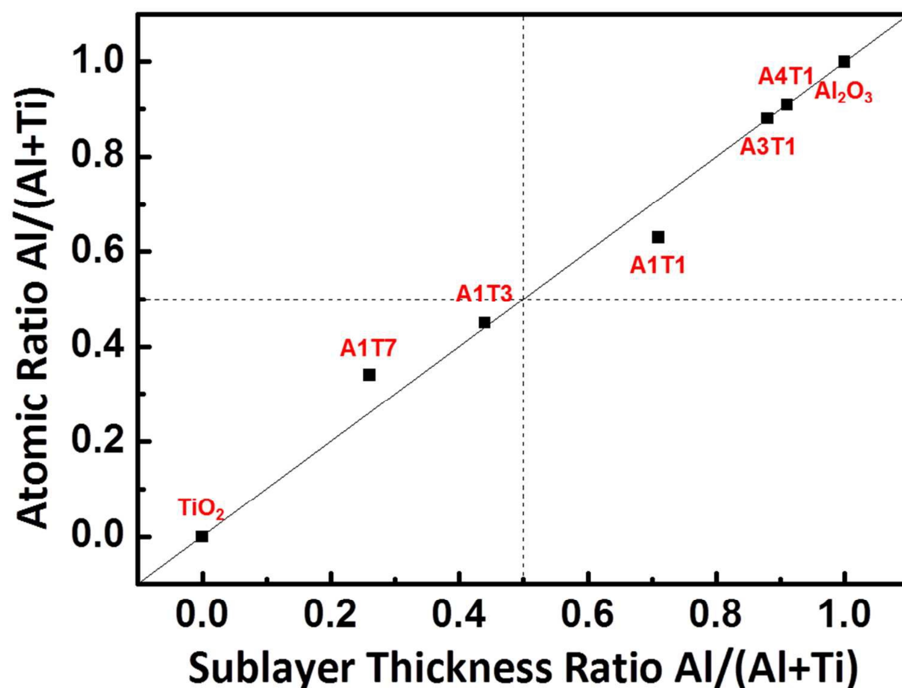

Figure 1. Comparison of the atomic ratio and sublayer thickness ratio in the PEALD-based films grown at 100˚C.

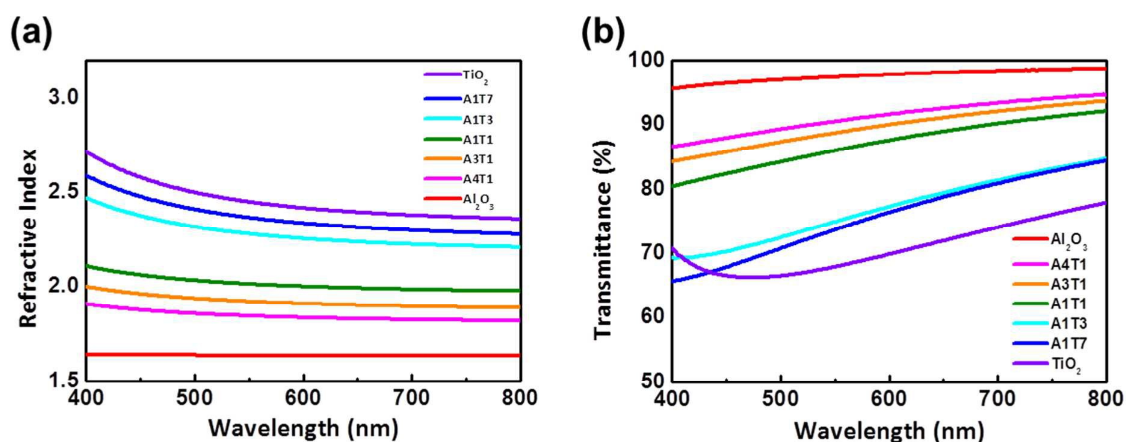

Figure 2. (a) The refractive index and (b) transmittance of PEALD-based films prepared with a thickness of 50 nm.

Physical Chemistry Chemical Physics Accepted Manuscript

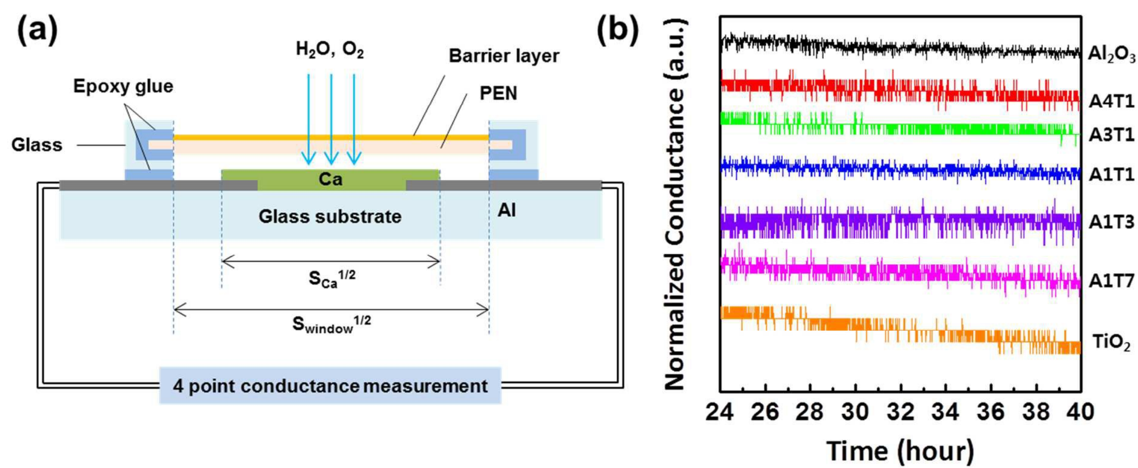

Figure 3. (a) Schematic diagram showing the Ca test, and (b) normalized conductance changes in the Ca encapsulated with PEALD films on a PEN substrate at 60˚C and 90% RH.

Physical Chemistry Chemical Physics Accepted Manuscript

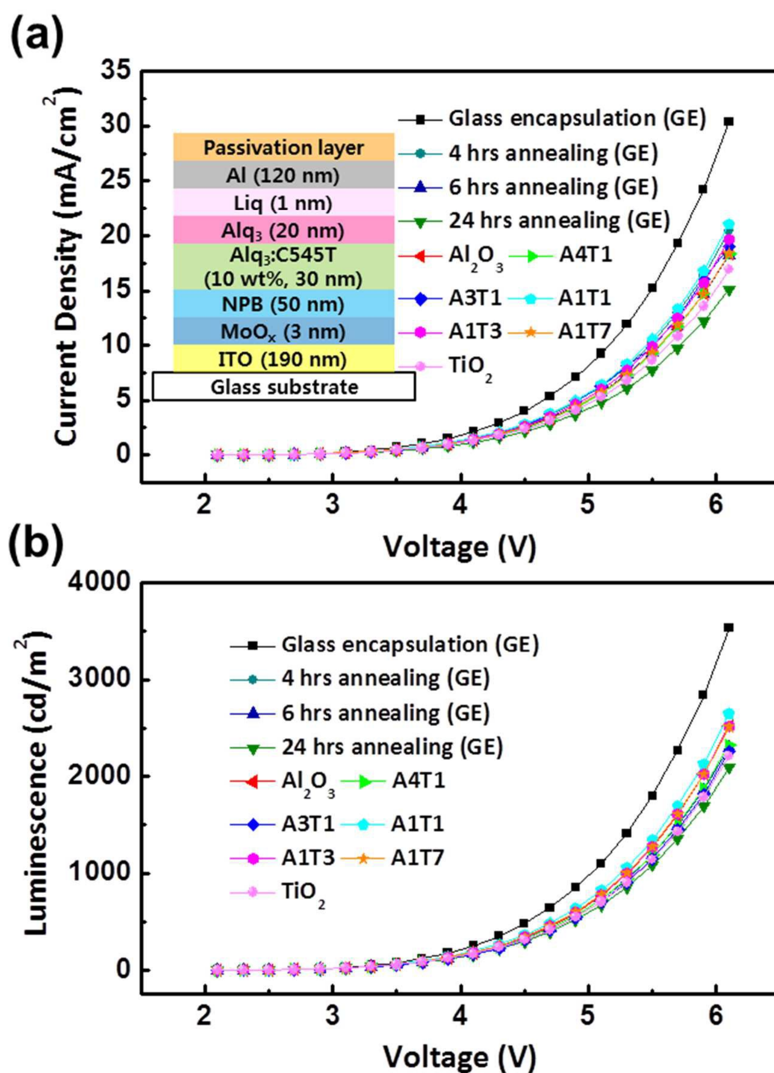

Figure 4. (a) *J-V* and (b) *L-V* characteristics of the OLED devices prepared with PEALD-based passivation layers and glass-encapsulated devices. The inset shows a schematic configuration of OLED.

Physical Chemistry Chemical Physics Accepted Manuscript

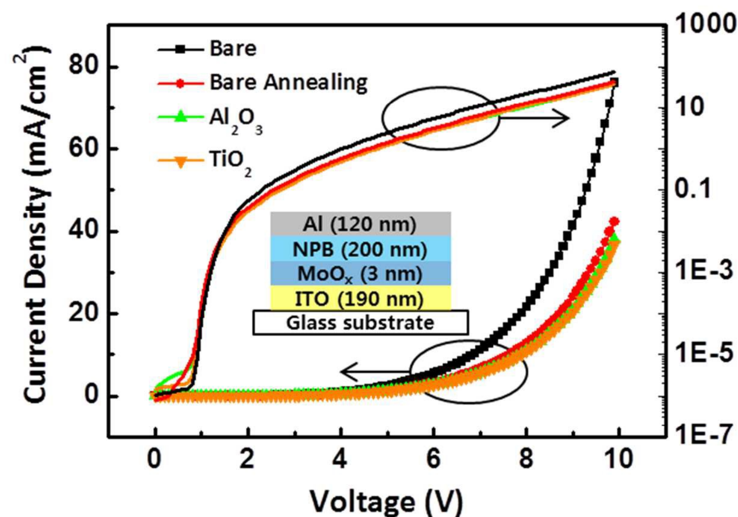

Figure 5. *J-V* characteristics of hole-only devices prepared with and without PEALD-based passivation layers. The inset shows a schematic configuration of hole-only device.

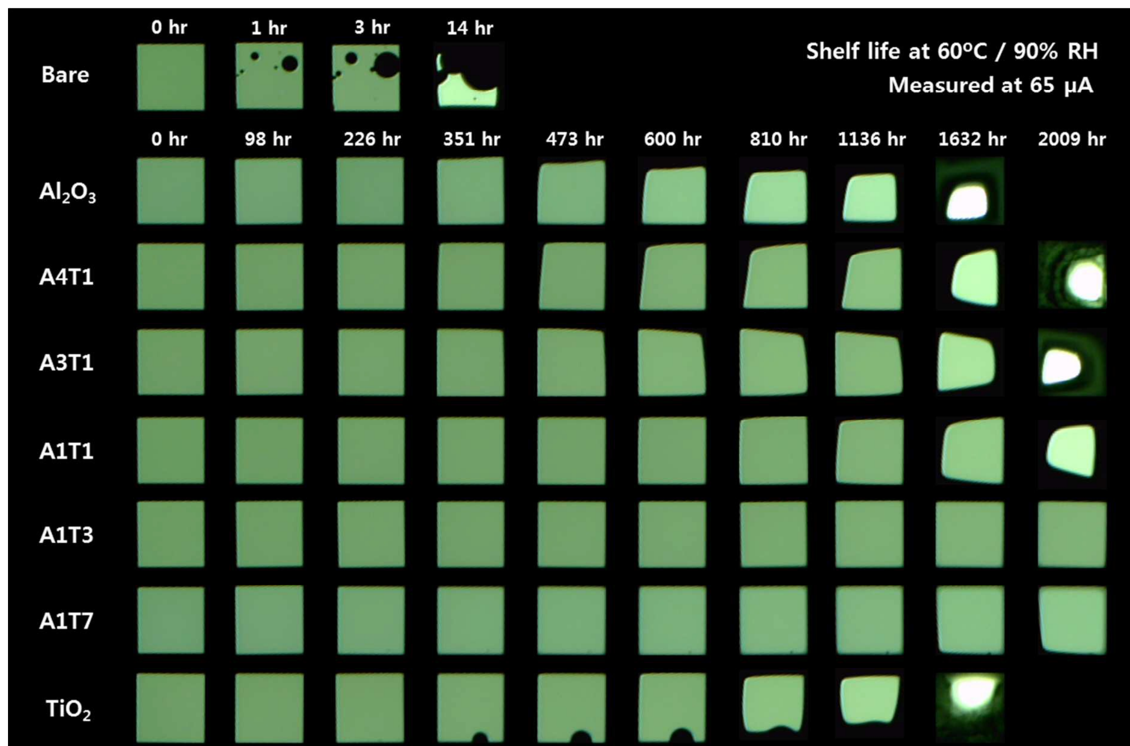

Figure 6. Shelf-life of the OLED devices passivated with and without PEALD-based films at

Physical Chemistry Chemical Physics Accepted Manuscript

60˚C and 90% RH.

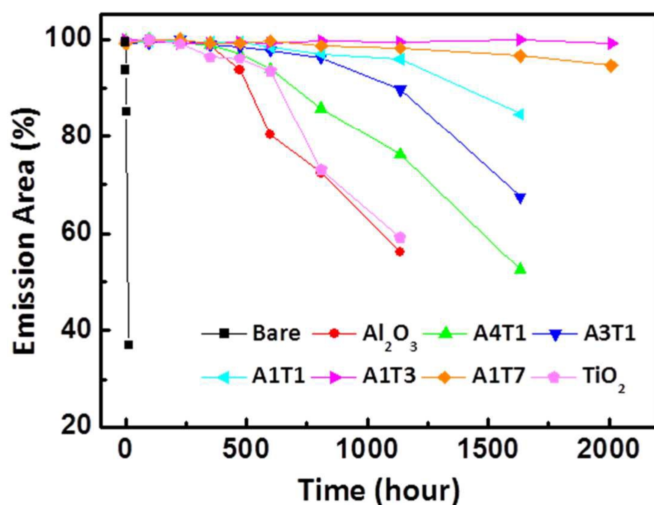

Figure 7. Emission area over time, measured in OLED devices passivated with or without PEALD-based films at 60˚C and 90% RH.

Table 1. Refractive index at 550 nm, the average optical transmittance across the visible region (400 nm–800 nm), and WVTR values of the PEALD-based films.

Materials	Refractive Index	Transmittance (%)	WVTR (g m^{-2} day^{-1})	Note
Al_2O_3	1.6370	97.63	3.69×10^{-4}	Single Al_2O_3 film
A4T1	1.8456	91.25	2.70×10^{-4}	(Al_2O_3 7.2 Å / TiO_2 0.75 Å) x 63
A3T1	1.9214	89.60	2.29×10^{-4}	(Al_2O_3 5.4 Å / TiO_2 0.75 Å) x 81
A1T1	2.0141	87.09	1.53×10^{-4}	(Al_2O_3 1.8 Å / TiO_2 0.75 Å) x 196
A1T3	2.2816	76.96	9.16×10^{-5}	(Al_2O_3 1.8 Å / TiO_2 2.25 Å) x 123
A1T7	2.3366	75.76	2.92×10^{-4}	(Al_2O_3 1.8 Å / TiO_2 5.25 Å) x 71
TiO_2	2.4501	70.80	6.52×10^{-4}	Single TiO_2 film

Physical Chemistry Chemical Physics Accepted Manuscript